RESEARCH ARTICLE

Reduced dorsal CA1 activity limits retention of the temporal component of declarative memory in the *Cntnap2* knockout mouse model of autism

Elise Caitlin Rawlinson[1], Michael Hugh McCullough[1,2], Azza Sellami[3,4], Aline Marighetto[3,4], Alice Shaam Al-Abed[1,5*†], Nathalie Dehorter[1,5*†]

[1]Eccles Institute of Neuroscience, John Curtin School of Medical Research, The Australian National University, Canberra, Australia; [2]School of Computing, The Australian National University, Canberra, Australia; [3]Neurocentre Magendie, Physiopathologie de la plasticité neuronale, U1215, INSERM, Bordeaux, France; [4]Université de Bordeaux, Bordeaux, France; [5]The Queensland Brain Institute, The University of Queensland, Brisbane, Australia

***For correspondence:** shaam.alabed@anu.edu.au (ASA-A); n.dehorter@uq.edu.au (ND)

[†]These authors contributed equally to this work

Competing interest: The authors declare that no competing interests exist.

Funding: See page 16

Preprint posted
05 May 2026
Sent for Review
28 May 2026
Reviewed preprint v1
14 August 2026
Reviewed preprint v2
28 September 2026
Version of Record
13 October 2026

Reviewing Editor: Laura A Bradfield, The University of Sydney, Australia

© Copyright Rawlinson *et al.* This article is distributed under the terms of the Creative Commons Attribution License, which permits unrestricted use and redistribution provided that the original author and source are credited.

eLife Assessment

This **important** study uses the *Cntnap2* mouse model of autism to investigate how reduced activity in the dorsal CA1 region of the hippocampus contributes to impaired temporal binding and memory flexibility. The authors combined trace conditioning and radial maze assays with fibre photometry, optogenetic rescue, and brain-wide c-Fos mapping to provide **convincing** evidence that dorsal CA1 hypoactivity limits the retention of temporally separated associations and biases learning towards less flexible strategies. The work advances understanding of hippocampal contributions to cognitive alterations associated with autism and will be of broad interest to researchers studying memory, hippocampal function, and neurodevelopmental disorders.

Abstract Growing evidence implicates the hippocampus in the pathophysiology of autism spectrum disorder, particularly in the domains of social interactions and cognition. Yet, the mechanisms driving the hippocampal-dependent cognitive atypicalities in autism remain poorly defined. Here, we characterized how dysfunction of the CA1 subfield of the dorsal hippocampus drives abnormalities in critical components of declarative memory. Using trace fear conditioning in the *Cntnap2* knockout mouse model of autism, we found that capabilities to retain the association of temporally distant stimuli (i.e. temporal binding) were reduced relative to wildtype mice. Fiber photometry and optogenetic experiments demonstrated that reduced CA1 activity during temporal gaps underlies this impairment, linking CA1 dysfunction to a deficit in long-term memory retention in autism. Using a relational/declarative memory task, we also revealed a deficit in flexible spatial memory, and a preferential use of egocentric learning strategy. This inflexible learning strategy resulted from an imbalance between memory system activity, promoting frontostriatal-dependent procedural learning instead of dorsal CA1/hippocampus-dependent relational/declarative memory. Overall, this study establishes dorsal CA1 dysfunction as a circuit-level mechanism underlying cognitive inflexibility in autism, providing a neurobiological framework for hippocampal-dependent memory deficits in the condition.

Introduction

Autism spectrum disorder (ASD) is a lifelong neurodevelopmental disorder comprising difficulties in social behavior, atypical communication skills, and the presence of restricted or repetitive behaviors or interests (DSM-5 and ***Association American Psychiatric, 2013***). Beyond these core features, individuals with ASD present with difficulties in cognitive domains that can impact daily functioning and adaptability. In particular, people with ASD present with atypicalities in episodic/declarative memory (***Bal et al., 2015***), the ability to recall specific events and experiences (i.e. *what happened, when, and where*). However, the underlying neurological mechanisms of declarative memory impairments in ASD have yet to be fully elucidated.

While most research has focused on the dysregulation of the prefrontal cortex and the basal ganglia in ASD, recent studies have highlighted that hippocampal defects are key to the social domain of this phenotype (***Banker et al., 2021***). In addition, the hippocampus is known to play a critical role in declarative memory by forming temporally and spatially organized relational representations of past experiences, allowing flexible expression of memories (***Eichenbaum, 2004***). The CA1 subfield plays a key role in this relational process by sustaining the ability to link temporally distant events, known as temporal binding (***Eichenbaum, 2014***; ***Sellami et al., 2017***). In autistic individuals, difficulties in the binding of episodic memories have been proposed in autistic individuals while memory for items alone remains relatively spared, positing a selective weakness in hippocampus-dependent linking of items and contexts (***Bowler et al., 2011***; ***Minor et al., 2023***). In parallel with this relational hypothesis of memory defects, time estimation tasks in individuals with ASD have shown that disruptions in integrating temporal information affect the development of temporal relationships (***Buonomano et al., 2023***; ***Maister and Plaisted-Grant, 2011***; ***Vogel et al., 2022***). In this context, we hypothesized that CA1 activity underlying temporal processing and temporal linking is impaired in ASD, leading to declarative memory defects.

Here, we examined this hypothesis in the *Cntnap2* knockout (KO) mouse model of ASD, which exhibits autism-like phenotypes, including social behavior deficits (***Peñagarikano et al., 2011***; ***Peñagarikano and Geschwind, 2012***), hippocampal alterations, and CA1 circuit-level changes and impairments in spatial discrimination (***Paterno et al., 2021***). Animals were assessed in two behavioral paradigms: trace fear conditioning (***Pavlov, 1927***; ***Sellami et al., 2017***), a simple temporal binding-dependent memory task allowing the simultaneous recording and manipulation of CA1 activity; and a radial maze task modeling the complexity of temporal binding-dependent relational/declarative memory (R/DM). We demonstrate that *Cntnap2* KO mice present with mistuned dCA1 activation and abnormal reorganization of memory systems during temporal binding-dependent memory formation.

Results

Cntnap2 KO mice demonstrate reduced temporal binding capability

We tested the temporal binding capabilities of the *Cntnap2* KO mouse model using the trace fear conditioning paradigm (TFC; ***Figure 1A***), in which mice are required to memorize the association between a tone (conditioned stimulus) and a mild electric foot-shock (unconditioned stimulus), separated by a temporal gap. Successful conditioning across this gap is thought to depend on the organism maintaining a decaying memory representation, or *trace*, of the CS after its offset; accordingly, this gap is conventionally termed the trace interval, and the paradigm trace conditioning (***Pavlov, 1927***; ***Sellami et al., 2017***). In the conditioning stage, independent groups of mice were exposed to three tone-shock pairings with a trace interval between 5 and 40 s (i.e. T5, T20, or T40; ***Figure 1A***). All groups showed intact conditioning abilities, demonstrated by high and increasing freezing times (***Blanchard et al., 1986***) during the tones and traces periods (***Figure 1B***, ***Figure 1—figure supplement 1A***). Twenty-four hours later, the animals were re-exposed to the conditioned *tone* in a neutral context (i.e. tone test) to assess 24 hr retention capacities of the tone-shock association. Retention was reflected in fear responses to the tone and trace compared with before and after the tone (i.e. conditioned fear response in ***Figure 1C***, % time freezing in ***Figure 1—figure supplement 1B***). Elevated freezing during the pre-tone period at T40 may reflect fear generalization (***Figure 1—figure supplement 1B***, T20 vs. T40 ***Sellami et al., 2017***). Interestingly, *Cntnap2* KO mice also displayed a strong and specific freezing response to the tone for up to a 20 s trace interval (***Figure 1C***, T20), but not for 40 s (***Figure 1C***, T40; ***Figure 1—figure supplement 1B***, T40). The animals were then exposed to the conditioning *context*

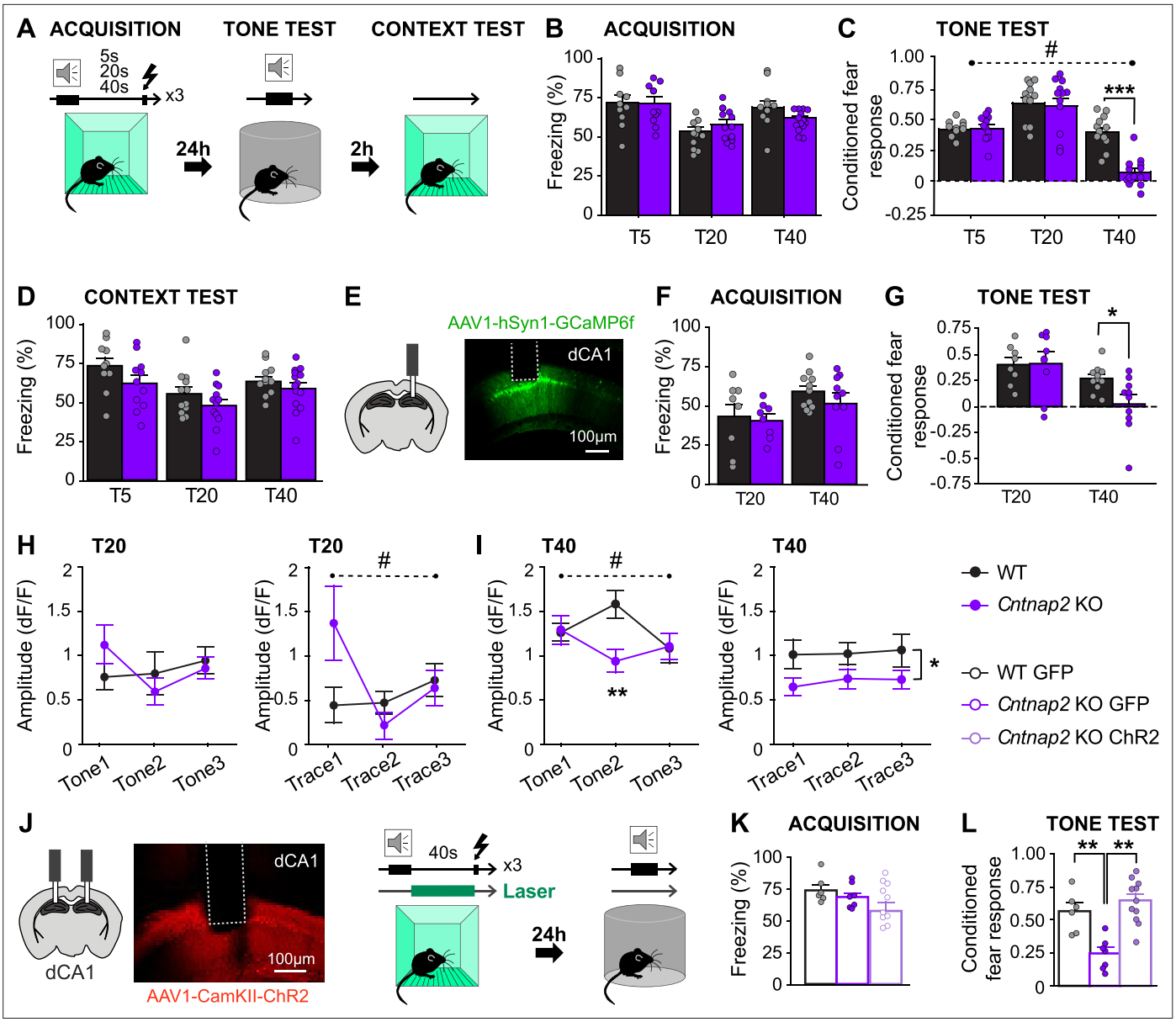


Figure 1. Reduced retention of temporal associations is associated with altered calcium responses during trace fear conditioning acquisition in *Cntnap2* KO mice. (**A**) Experimental design: Trace Fear Conditioning includes a conditioning session in which mice have to associate a tone and a shock, separated by a time interval (trace). Independent groups of mice were trained with trace intervals of 5, 20, or 40 s. (**B**) Freezing levels (percent) during the third tone of the conditioning session for WT (black) and *Cntnap2* KO (purple) groups, conditioned with distinct trace durations (T5: WT n=10; *Cntnap2* KO n=11; T20: WT n=12; *Cntnap2* KO n=11; T40: WT n=12; *Cntnap2* KO n=14). (**C**) Conditioned fear response during the tone test (i.e. ratio of freezing before the tone compared to during the tone and the trace, see methods), 24 hr post-conditioning with distinct trace durations (Genotype X Trace interaction: $F_{2,65}$=11.278; p<0.0001; T40: Genotype: $F_{2,24}$=6.944; p=0.0163). (**D**) Freezing levels in the conditioning context (context test) for WT (black) and *Cntnap2* KO (purple) groups, 24 hr post-conditioning. (**E**) *Fiber photometry*. Left: scheme depicting the fiber optic implantation targeting the dorsal CA1 subfield of the hippocampus (dCA1). Right: Representative image of the optic fiber placement, in the pyramidal cell layer of the dCA1, scale: 100 µm. Calcium activity was recorded using the calcium indicator GCaMP6f (green). (**F**) Freezing levels (percent) during the third tone of the conditioning session for WT (black) and *Cntnap2* KO (purple) groups, conditioned with distinct trace durations (T20: WT n=8; *Cntnap2* KO n=8; T40: WT n=11; *Cntnap2* KO n=10). (**G**) Conditioned fear response during the tone test (i.e. ratio of freezing before the tone compared to during the tone and the trace, see Materials and methods), 24 hr post-conditioning with distinct trace durations (T40: Genotype: $F_{1,19}$=50.143; p<0.0001). (**H**) Left: Peak amplitude of Ca^{2+} transients during the three tone presentations of the conditioning under a 20 s trace-interval (ns). Right: Peak amplitude of Ca^{2+} transients during the three trace intervals of the conditioning under a 20 s trace-interval (Genotype x Trace interaction: p=0.0476; WT n=8; KO n=8, trace 1: ns (p=0.0675)). (**I**) Left: Peak amplitude of Ca^{2+} transients during the three tone presentations of the T40 conditioning session (Genotype x Tone interaction: p=0.0247; Tone: p=0.0053; WT n=11; KO n=10). Right: Peak amplitude of Ca^{2+} transients during the three trace intervals of the T40 conditioning session (Genotype: p=0.0408; WT n=11; KO n=10). (**J**) *Optogenetics*: Left panel: scheme depicting the fiber optic implantations bilaterally

Figure 1 continued on next page

Figure 1 continued

targeting the dorsal CA1 subfield of the hippocampus (dCA1). Right panel: Representative image of the optic fiber placement, in the pyramidal cell layer of the dCA1, scale: 100 µm. Pyramidal neurons' activity was manipulated only during the trace interval using Channel Rhodopsin (ChR2). (**K**) Freezing levels (percent) during the third tone of the conditioning session for GFP-injected WT (black, n=6), GFP-injected *Cntnap2* KO (purple, n=7), and ChR2-injected *Cntnap 2* KO (light purple/white, n=11) groups, conditioned with 40 s trace duration. (**L**) Conditioned fear response during the tone test (i.e. ratio of freezing before the tone compared to during the tone and the trace, see Materials and methods), 24 hr post-conditioning with distinct trace durations (Groups: $F_{2,21}$=15.576; p<0.0001; WT-GFP *vs* KO-GFP: p=0.0010; KO-GFP *vs* KO-ChR2: p<0.0001). Data shown at mean ± SEM. *: p<0.05; **: p<0.01; ***: p<0.001; * represents genotype effect, determined by student's t-test. # represents genotype x variable interaction, determined by two-wayANOVA, followed by Bonferroni post-hoc.

The online version of this article includes the following figure supplement(s) for figure 1:

Figure supplement 1. Freezing levels and calcium peak frequencies during the fiber photometry recordings (***Figure 1***).

alone to evaluate contextual memory. As previously demonstrated (***Al Abed et al., 2020b***; ***Sellami et al., 2017***), WT mice displayed efficient retention of the tone-shock association up to a 40 s trace interval, illustrated by a strong and specific conditioned fear response to the tone in a neutral context (***Figure 1D***). These results were replicated in both control and *Cntnap2* KO littermates (***Figure 1—figure supplement 1C***). Altogether, these results indicate that *Cntnap2* KO mice exhibit reduced temporal binding capacity compared to WT mice, which compromises the 24 hr retention of the tone-shock association.

As freezing is the absence of movement, the well-reported hyperlocomotion in *Cntnap2* KO mice (***Peñagarikano et al., 2011***; ***Figure 1—figure supplement 1D***) could represent a potential confounding factor. However, we observed comparable levels of resting time (***Figure 1—figure supplement 1D***, right panel) and similar freezing levels between WT and *Cntnap2* KO mice during acquisition, regardless of the trace interval (***Figure 1—figure supplement 1A***), as well as during memory tests under control conditions (***Figure 1—figure supplement 1B***; T5, T20, and T40). These findings indicate that locomotor activity alone cannot account for the observed differences in freezing. Taken together, our results demonstrate that *Cntnap2* KO mice exhibit reduced temporal binding capacity during conditioning, which does not affect acquisition but impairs the 24 hr retention of the tone-shock association.

Mistuning of dorsal CA1 activity during temporal binding in *Cntnap2* KO mice

Whilst alterations in item binding in ASD have already been reported, the underlying mechanisms have not been described (***Minor et al., 2023***). As the sustained activity of dCA1 neurons during time intervals between stimuli is necessary for long-term retention of their association (***Al Abed et al., 2020b***; ***Sellami et al., 2017***), we examined dCA1 activity during acquisition in *Cntnap2* KO mice. We recorded calcium transients during encoding and recall of trace fear conditioning, using fiber photometry in animals trained under a 20 s or 40 s-trace interval (***Figure 1E***). Both WT and *Cntnap2* KO mice implanted with an optic fiber could acquire the tone-shock association, reaching high levels of freezing after three tone-shock pairings (***Figure 1F***, ***Figure 1—figure supplement 1E***). During conditioning, in both T20 and T40 conditions, regardless of genotype, the frequency of the calcium transients in response to the tone significantly decreased across tone presentations, suggesting neural adaptation to successive tone exposure (***Figure 1—figure supplement 1F, G***). *Cntnap2* KO mice trained under the 20 s trace interval displayed no difference compared to WT in the frequency of calcium transients during the tone and the trace interval (***Figure 1—figure supplement 1F***), while the amplitude tended to be higher during the first trace interval in Cntnap2 KO mice (***Figure 1H***). In the 40 s trace-conditioned group, the frequency of the calcium transients did not differ between WT and C*ntnap2* KO mice throughout conditioning (***Figure 1—figure supplement 1G***). In contrast, the calcium transient *amplitude* was significantly reduced both during the presentation of the second tone (***Figure 1I***, left) as well as throughout the three trace intervals in *Cntnap2* KO mice (***Figure 1I***, right). Overall, these results suggest a lack of synchronized neuronal activity during encoding, as previously reported (***Simon and Wallace, 2016***). During the tone test, as in ***Figure 1C***, *Cntnap2* KO mice displayed appropriate retention of the tone-shock association when conditioned under a 20 s-trace interval while the ones trained under a 40 s-trace interval failed to express a fear response to the tone (***Figure 1—figure supplement 1H, I***). This indicates impaired retention of trace fear memory and

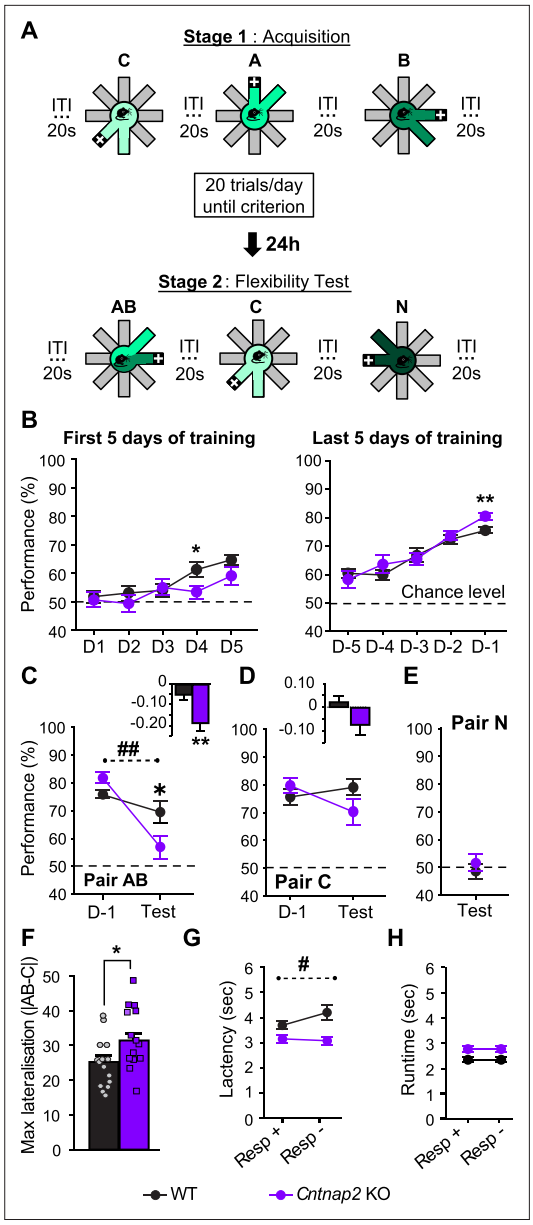


Figure 2. *Cntnap2* KO mice display impaired relational/declarative memory. (**A**) Experimental design: Relational/Declarative memory task. ITI: Inter-trial interval; +: represent reward location within each pair of arms. (**B**) Average correct answers for WT (black; n=15) and *Cntnap2* KO mice (purple; n=14) for pairs A, B, and C during the first 5 days of acquisition (left panel; day (**D**); D4: Genotype: p=0.0149), and the last 5 days of acquisition (right panel; D-5: 5 days before they reach learning criterion; D-1: Genotype: p=0.0082). (**C**) Comparison of the correct answers during the last day of training (D-1) averaged on pairs A and B, and during the flexibility test on the recombined pair AB (Genotype X Performance interaction: $F_{1,27}$=12.639, p=0.0014; Test, Genotype: p=0.0239). Inset: D-1 *vs.* Test performance index on pairs AB (Genotype: p=0.0022). (**D**) Comparison of the correct answers on pair C during

Figure 2 continued on next page

temporal binding ability, relative to WT mice. The findings also suggest that sustained activity of dCA1 neurons during encoding of the three trace intervals, which is higher in WT than in *Cntnap2* KO mice, supports temporal binding and enables adequate retention of the association between the 40 s-distant tone and shock despite their temporal separation without affecting initial acquisition. These results further support the idea that the reduction in temporal binding capacity in *Cntnap2* KO mice stems from a lack of sustained dCA1 activity during encoding and recall of the tone-shock association.

In WT mice, we have previously demonstrated that the activity of dCA1 principal neurons during the trace interval (but not outside of the trace interval) is required for long-term retention, but not for encoding of temporal associations (***Sellami et al., 2017***). To further confirm a causal link between sustained dCA1 activity during temporal gaps and 24 hr retention in *Cntnap2 KO*, we optogenetically activated principal neurons specifically during the 40 s trace interval of the conditioning session using ChannelRhodopsin (ChR2; ***Figure 1J***), while leaving neuronal activity unaltered during the remainder of acquisition and the 24 hr test. During the conditioning session, all groups displayed increased freezing across the three tone-shock pairings, indicative of efficient acquisition (***Figure 1K***, ***Figure 1—figure supplement 1J***). Twenty-four hours later, ChR2-expressing *Cntnap2* KO mice demonstrated a specific freezing response to the tone and trace, unlike GFP-expressing *Cntnap2* KO mice (***Figure 1L***, ***Figure 1—figure supplement 1K***). These results demonstrate that dCA1 neuronal activity during trace intervals drives temporal binding in *Cntnap2* KO mice.

Egocentric learning and inflexible long-term memory in *Cntnap2* KO mice

Following the observation that *Cntnap2* KO mice present reduced dCA1 activity associated with temporal binding capabilities, we examined potential atypicalities in declarative memory. We used a radial maze task that models the complexity of temporal binding-dependent relational/declarative memory (R/DM; ***Sellami et al., 2018***). This task assesses the characteristic flexibility of R/DM expression, which relies on the dCA1-dependent ability to relate temporally distant events (***Sellami et al., 2017***).

To do so, the R/DM task is divided into two stages: an acquisition phase and a flexibility test

Figure 2 continued

the last day of training (D-1) and the flexibility test. Inset: D-1 *vs.* Test performance index for Pair C. (**E**) Average performance on the new pair N during the flexibility test. (**F**) Maximum lateralization index during stage 1 (absolute value of the average performance between pairs A and B (left baited) minus Pair C (right baited); Genotype: p=0.0153). (**G**) Average decision latencies for correct (+) and incorrect (-) answers throughout training (Genotype X Response interaction: $F_{1,31}$=7.960, p=0.0083). (**H**) Average runtimes for correct (+) and incorrect (-) answers throughout training (Resp -, Genotype: p=0.0500). Dashed line illustrates chance level. Data shown at mean ± SEM. *: p<0.05; **: p<0.01; # shows genotype x performance interaction, determined by two-wayANOVA, followed by Bonferroni post-hoc.

(***Figure 2A***). In the acquisition stage, mice are trained daily to learn the food-reward location within three separate pairs of adjacent arms. Critically, this task structure requires mice to encode each pair as a distinct, temporally separated experience, rather than allowing continuous comparison between pairs. Cumulative evidence shows that declarative flexibility relies on a hippocampus-dependent relational representation of separate experiences formed for each pair during the acquisition phase (***Al Abed et al., 2020b***; ***Mingaud et al., 2007***; ***Sellami et al., 2017***). After reaching the learning criterion (>75% correct choices of the rewarded arm), declarative memory is then probed by testing whether animals can recombine two of these separately learned pairs (A and B) into a novel configuration (pair AB) without any change to the reward location (***Figure 2A***). Successful performance requires that the two pairs were encoded relationally, within a shared spatial representation, allowing this new relation to be inferred; poor performance, in contrast, suggests animals relied on rigid, pair-specific response rules that do not generalize to novel arm combinations. To impose a temporal binding demand on relational memory acquisition, the presentation of each pair is separated by a 20 s intertrial interval. This timing was empirically determined in ***Sellami et al., 2018***; ***Sellami et al., 2017***.

Both wild-type (WT) and *Cntnap2* KO mice were able to acquire the task (***Figure 2B***). *Cntnap2* KO mice tended to require more days to reach criterion (average number of days: WT: 8.06, KO: 10.86, ns, raw data in ***Source data 1***) and reached higher performance levels at the end of training (***Figure 2B***, right panel).

In the flexibility test, their performance dropped significantly between the last training session and the flexibility test (stage 2 of the R/DM task), and *Cntnap2* KO mice performed significantly worse than WT (***Figure 2C*** - Recombined pair AB). In contrast, both groups performed similarly on the control pairs: the unchanged pair C, with high performance (***Figure 2D***), and the novel pair N, at chance levels (***Figure 2E***).

What could explain this lack of flexibility? We have previously shown that the flexibility component of R/DM depends on the learning strategy used during the acquisition stage: either allocentric spatial mapping (relational) or egocentric (procedural), the latter leading to lateralization. Indeed, when the use of spatial cues is impaired, as in cases of hippocampal damage or dysfunction, mice adopt a left-right egocentric strategy to memorize reward locations leading to inflexible memory (***Mingaud et al., 2007***; ***Sellami et al., 2017***). Therefore, the chance-level flexibility performance of *Cntnap2* KO mice suggests a bias towards a procedural learning strategy, in line with the well-documented prominence of behavioral inflexibility (***Uddin et al., 2015***) and the use of egocentric learning strategies in ASD (***Brunner et al., 2015***; ***Ring et al., 2018***). This was confirmed by analyzing lateralization during acquisition by comparing performance on left-baited pairs (pairs A and B), *vs.* right-baited pair C (Materials and methods, ***Figure 2F***). *Cntnap2* KO mice displayed significantly more lateralization than WT, meaning they used an egocentric/procedural strategy to learn the position of the food reward rather than using the spatial mapping strategy observed in WT mice. We found no significant correlation between the use of egocentric strategy and the number of days to reach criterion (Data in Figure S3). Notably, performance during Day 4 of acquisition in WT mice was significantly negatively correlated with their use of lateralized strategy (r^2=–0.518, p=0.0471), which was not seen in *Cntnap2* KO mice. Together, this further confirms that *Cntnap2* KO mice employ a lateralized strategy to learn the task, which impacts both task performance (***Figure 2B***, day 4) and memory flexibility (***Figure 2C***).

Interestingly, *Cntnap2* KO mice had shorter decision times than WT (***Figure 2G***), consistent with the well-demonstrated impulsivity observed in ASD (DSM-5 and ***Association American Psychiatric, 2013***). In addition, WT mice demonstrated a longer time to enter a non-baited arm than a baited arm, suggesting that they evaluate reward location before entering the arm, likely relying on deliberation

and precise spatial representation. In contrast, *Cntnap2* KO mice showed similarly short latencies regardless of their choice, suggesting impulsive, automatic responses and impaired spatial representation of reward information. In addition, once a choice was made, their running time (from the central platform to the end of the arm) was longer than that of WT mice (***Figure 2H***), implying that while the deliberative phase is shortened or absent in KO mice, there may be a compensatory adjustment following impulsive decisions.

Altogether, these findings indicate that *Cntnap2* KO mice exhibit impaired flexible memory expression, consistent with a relational/declarative memory deficit and increased reliance on an egocentric/procedural learning strategy.

Potential shift toward striatum-centered activities in *Cntnap2* KO mice

Each learning strategy is known to depend on partially distinct brain systems: hippocampus-dependent systems supporting allocentric spatial/relational learning, and striatum-based systems leading to egocentric/procedural learning (***White and McDonald, 2002***). To assess learning-induced activity in these different structures, we quantified the levels of the cellular activity marker cFos after day 3 of R/DM task acquisition in structures involved in memory (i.e. the dorsal hippocampus [dCA1, dCA2, dCA3, the dorsal dentate gyrus (dDG)]; the dorso-medial (DMS) and the dorso-lateral striatum (DLS); the prefrontal cortex [infralimbic (IL), prelimbic (PrL), and anterior cingulate (ACC)]; ***Figure 3A***, ***Figure 3—figure supplement 1***).

As previously shown (***Al Abed et al., 2020b***; ***Sellami et al., 2017***), we found a significant activation of dCA1 in trained WT mice compared to naïve WT mice (***Figure 3B***), consistent with the use of an allocentric/spatial learning strategy (***White and McDonald, 2002***). In contrast, *Cntnap2* KO mice showed no learning-induced dCA1 activation (***Figure 3B***), together with hypoactivation of dCA3 in both naïve and trained groups compared to WT mice (***Figure 3—figure supplement 1A***). This reduced hippocampal activation may contribute to the observed deficit in temporal binding and spatial learning capabilities in this task. Moreover, *Cntnap2* KO mice displayed a significant training-induced activation of the DMS compared to their naïve controls, a pattern not observed in WT mice (***Figure 3C***). No other significant changes were detected in the hippocampus (i.e. dCA2, DG; ***Figure 3—figure supplement 1A***), in the DLS (***Figure 3—figure supplement 1B***) or in the prefrontal cortex regions (i.e. IL, PrL, ACC; ***Figure 3—figure supplement 1C***). Together, these findings suggest increased engagement of DMS-associated networks during the egocentric learning strategy adopted by *Cntnap2* KO mice.

To further dissect the balance between memory systems, we analyzed the relative contribution of each structure within the total activation of the system (***Figure 3D–E***). After training, we found a disproportionate representation of the PFC and striatum relative to the hippocampus in *Cntnap2* KO mice compared to WT (***Figure 3D***). Indeed, compared to WT naïve mice, WT trained mice exhibited an increase in the weight of the dCA1 in the network activity, likely supporting temporal binding and, through ensuing relational organization of the 20s-distant pair presentations, the formation of flexible memory. In contrast, no such reorganization of network activity was observed in *Cntnap2* KO mice with training (***Figure 3E***). We observed differences in the relative contribution of individual substructures between trained WT and *Cntnap2* KO mice. Specifically, training was associated with greater involvement of the dCA1, dCA2, and dCA3 in WT mice, whereas *Cntnap2* KO mice showed greater involvement of the DMS, IL, and ACC. Overall, we observed compensatory activation of the frontal-striatal structures concomitant with hippocampal hypoactivation in the *Cntnap2* KO model.

In addition to the learning-induced activity of individual structures, pairwise correlation of activity between structures enhances our understanding of network-wide synchronization. While naïve WT mice exhibited mainly positive correlations between the striatum, PFC, and hippocampus, with the exception of the dDG which was negatively correlated with the PFC, naïve *Cntnap2* KO mice displayed predominantly negative correlations (***Figure 3F***).

This indicates that, at baseline, inter-structural relationships are dysregulated in *Cntnap2* KO mice, potentially limiting the recruitment of a hippocampus-based learning strategy. Altogether, the analysis of learning-induced brain activity suggests a shift toward striatum-centered activity and connectivity in *Cntnap2* KO mice, likely promoting an egocentric learning strategy and resulting in inflexible memory.

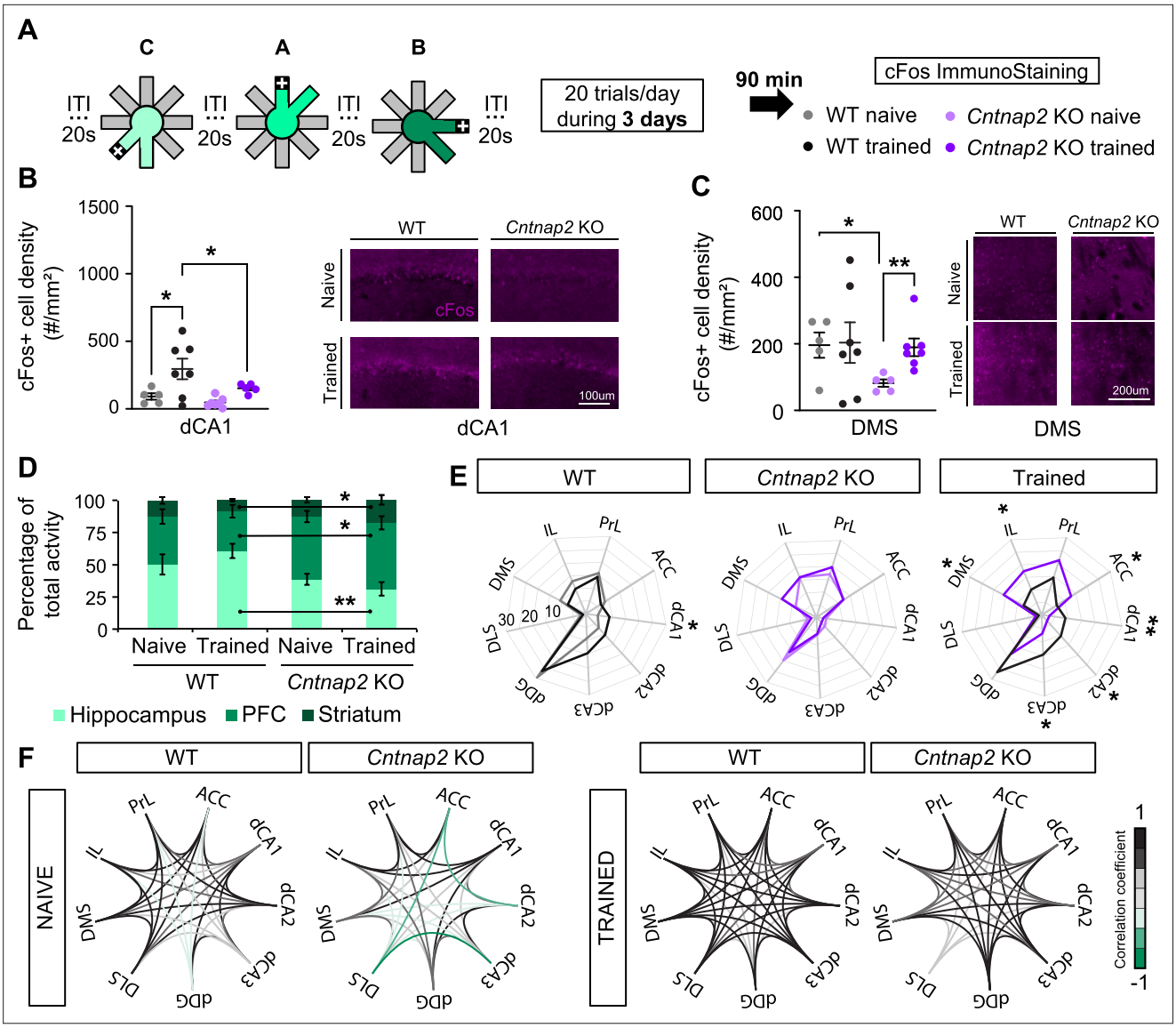


Figure 3. Learning-induced activity and functional connectivity in *Cntnap2* KO mice. (**A**) Experimental design: cFos levels were quantified 90 min after the 3rd training session of the Relational/Declarative memory task. ITI: Inter-trial interval; +represents reward location within each pair of arms (WT Naïve: n=5; WT Trained: n=7; *Cntnap2* KO: n=5; *Cntnap2* KO Trained: n=7). (**B**) Number of cFos-positive neurons (cell density/mm^2) in the dorsal dCA1 (WT naïve *vs* Trained: p=0.0491; Trained WT vs. KO: p=0.0129) with representative images of the cFos staining (Magenta) in dCA1, scale: 100 µm, for naïve (light colors) and trained (dark colors) WT (grey/black) and *Cntnap2* KO (purple) groups. (**C**) Number of cFos-positive neurons (cell density/mm^2) in the Dorso-Medial Striatum (DMS; Naïve WT vs. KO: p=0.0189; KO Naïve vs Trained: p=0.0085) with representative images of the cFos staining (Magenta) in DMS, scale: 200 µm. (**D**) Percentage of total activity: activity of each structure over to the total activity measured (percentage; Trained WT vs. KO: Hippocampus: p=0.00194; PFC: p=0.00107; Striatum: p=0.0382). (**E**) Percentage of total activity: activity each subfield within the total network, in WT mice (naïve vs trained, left panel; dCA1: p=0.0242), in *Cntnap2* KO mice (Naïve vs trained, middle panel), and in trained mice (WT vs *Cntnap2* KO mice, dCA1: p=0.009; dCA2: p=0.0174; dCA3: p=0.0274; ACC: p=0.0438; DMS: p=0.0350; IL: p=0.0267; PrL: p=0.0476; right panel, same data as in left and middle panels). (**F**) Pairwise between-structure correlation strength of cFos cell density. Data shown as mean ± SEM. *: p<0.05; **: p<0.01, ***: p<0.001. * represents genotype effect, determined by student's t-test.

The online version of this article includes the following figure supplement(s) for figure 3:

Figure supplement 1. cFos density in the hippocampus, striatum, and prefrontal cortex.

Discussion

This study establishes a novel mechanistic framework that builds on prior reports of hippocampal alterations in *Cntnap2* KO mice (***Paterno et al., 2021***). It demonstrates that compromised CA1 hippocampal activity during encoding disrupts temporal binding, which, by impairing the relational

processing of temporally distant events, leads to deficits in retention of declarative memory. Moreover, hippocampal dysfunction in *Cntnap2* KO mice appears to shift learning away from hippocampus-dependent strategies and toward egocentric strategies.

Interplay between hippocampus and striatum in memory deficits in *Cntnap2* KO mice

Individuals with ASD show atypicalities in declarative memory, characterized by impaired relational binding, that is the ability to link discrete items or events into a unified representation, while memory for individual items in isolation appears comparatively preserved (***Minor et al., 2023***). Because many real-world relations must be formed across a temporal gap (e.g. linking an event to its outcome, or one experience to another encountered later), we propose that this relational impairment may arise, at least in part, from a deficit in temporal binding: the hippocampus-dependent process of maintaining and integrating information across time to construct coherent, flexible memories.

Here, we demonstrate a reduction in dCA1-dependent temporal binding capacity in *Cntnap2* KO mice, which could contribute to the declarative memory impairment by disrupting the relational organization of temporally distant events. Indeed, in the trace fear conditioning experiments, *Cntnap2* KO mice showed efficient temporal binding with time intervals up to 20 s, compared with 40 s in WT mice, and this reduction was associated with a reduction of dCA1 activity during the encoding of the 40s-trace fear conditioning. Temporal integration of stimuli relies on hippocampal activity, in particular that of dCA1 (***Buzsáki and Tingley, 2018***; ***Chowdhury et al., 2005***; ***Sellami et al., 2017***; ***Tsien et al., 1996***). Similarly, we found an impaired activation of the dCA1 in *Cntnap2* KO mice during the acquisition of the Relational/Declarative Memory (R/DM) task (***Figure 3B***).

The lack of training-induced dCA1 activation likely prevents fine-tuned temporal integration of distant events, leading to flexibility deficits (***Chang and Gold, 2003***; ***Etchamendy et al., 2003***; ***Mingaud et al., 2007***; ***Sellami et al., 2017***). Moreover, analysis of broader memory systems' activity during encoding revealed an aberrant recruitment of the DMS in the *Cntnap2* KO mice, along with an altered pair-wise correlation between activation of related brain regions (***Figure 3F***). While WT mice exhibited predominantly positive correlations, *Cntnap2* KO mice showed negative correlations among the DLS, prefrontal cortex, and hippocampus. This pattern was also observed in naïve groups, suggesting that the bias in ASD toward lateralized learning strategy stems from baseline mistuning of functional connectivity between brain structures necessary for spatial learning in ASD.

This shift toward a striatum-centered system in ASD also implies a predominance of unconscious encoding, in which relations between items are acquired via stimulus-response associations, leading to inflexible, habit-like actions (***Ferbinteanu, 2016***). Whether the increased reliance on corticostriatal pathways reflects a compensatory adaptation to impaired hippocampal processing or a direct consequence of *Cntnap2* deficiency remains an open question. *Cntnap2* is broadly expressed across cortico-hippocampal and corticostriatal circuits and has been implicated in neuronal connectivity, synaptic function, and network synchronization (***Lazaro et al., 2019***; ***Scott et al., 2019***; ***Selimbeyoglu et al., 2017***). It is therefore possible that the altered engagement of corticostriatal networks observed here is not solely secondary to reduced hippocampal activity, but also reflects primary circuit alterations caused by the genetic mutation. Future studies directly examining corticostriatal activity and manipulating these circuits during learning will be required to disentangle primary genetic effects from compensatory network adaptations. However, additional mechanisms may contribute to the phenotype. *Cntnap2* KO mice exhibit other neural and behavioral alterations (***Peñagarikano et al., 2011***), including epileptic seizures and hyperlocomotion, suggesting that CA1 hypoactivity is likely only one of several factors influencing performance. Similarly, although previous work demonstrated that dCA1 activation rescues temporal binding only when delivered during the trace interval (***Sellami et al., 2017***), future studies should determine whether the same temporal specificity is maintained in the *Cntnap2* KO model.

Decoding spatial and temporal maps in the *Cntnap2* KO mouse model of autism

The CA1 region is recruited with other hippocampal areas to form and maintain spatial, temporal, and social maps, which are mental relational representations of our environment (***Barrientos and Tiznado, 2016***). CA1 neurons contribute to encoding and recalling spatial information, enabling individuals

to navigate and understand their surroundings. Specific 'time cells' create a temporal framework that supports episodic memory, encoding the passage of time and the prediction of future events (***Eichenbaum, 2014***). Recent research also suggests that CA1 contributes to social cognition through so-called 'social maps' which process and recall social information that is essential for effective social behavior and social dynamics (***Zhang et al., 2022***). Yet, little is known about how cognitive deficits evolve over time and their long-term effects in ASD. While the present study focused on dCA1 activation during acquisition to assess how dCA1 binds distinct stimuli into unified representations, future investigations directly examining the causal role of dCA1 activity in memory maintenance and retrieval (e.g. ArchT-mediated silencing during recall) will be essential for a comprehensive understanding of dCA1's role in memory processes in ASD, as well as for exploring how specific maps are formed and maintained in this condition.

The role of dCA1 in spatial representations has been profusely documented. Consistently, we recently demonstrated the central role of dCA1 in the maladaptive contextual encoding in post-traumatic stress disorder (PTSD), that is the degradation of declarative memory surrounding a highly stressful event (***Al Abed et al., 2020a***; ***Brewin, 2011***; DSM-5 and ***Association American Psychiatric, 2013***). Interestingly, growing evidence reports the propensity to develop PTSD in ASD (***Al Abed et al., 2024***; ***Rumball et al., 2020***), suggesting that reduced dCA1 activation may impact cognition beyond everyday learning. Together, these studies further underscore the hippocampus as a promising target to alleviate ASD pathophysiology.

To obtain a deeper understanding of the hippocampus computation underlying memory formation, we analyzed the correlation between neuronal dynamics and behavioral outcomes within the fear memory test. Fiber photometry recordings in the dCA1 showed that while WT mice displayed sustained hippocampal activity during the trace interval (***Figure 1I***), hippocampus-dependent memory systems were not similarly activated in the *Cntnap2* KO mice (***Figure 3B and E***). We also found a marked decrease in the amplitude of calcium transients in *Cntnap2* KO mice (***Figure 1I***). This profile was not observed when *Cntnap2* KO mice were trained within their capacity (i.e. 20 s trace interval; ***Figure 1H***). However, because fiber photometry provides a population-level measure of activity, it does not resolve the contribution of individual CA1 neurons or underlying cellular and synaptic mechanisms. Future studies using approaches with single-cell or subcellular resolution will be required to determine how these mechanisms contribute to the altered CA1 dynamics observed here.

Overall, these results suggest that the deficits in temporal binding and declarative memory originate from reduced hippocampal neuronal synchronization and dynamics. An additional possibility is that sustained CA1 activity during the trace interval is supported not only by recurrent network interactions but also by intracellular mechanisms within CA1 pyramidal neurons. Persistent dendritic calcium signaling and CaMKII-dependent processes, including dendritic, delayed, and stochastic CaMKII activation (***Jain et al., 2024***) and short-term associative plasticity of calcium dynamics (***Caya-Bissonnette et al., 2023***; ***Caya-Bissonnette and Béïque, 2024***), have been proposed to support prolonged information retention. Determining the relative contributions of these intracellular and circuit-level processes will require future investigations with single-cell and subcellular resolution, as the network-level approaches used in the present study did not allow us to distinguish whether the sustained activity observed here arises from these cellular mechanisms, recurrent circuit dynamics, or a combination of both. In the same line, a recent study reported that neurons allocated to the memory trace displayed freezing-specific activity compared to non-allocated neurons during contextual fear conditioning (***Mocle et al., 2024***). While our study design does not provide these details, the lack of active cells in the dCA1 during acquisition of the relational/declarative memory task could imply memory trace allocation to the striatum rather than the hippocampus (***Rashid et al., 2016***). Further experiments are needed to determine whether atypical engram allocation is linked to learning strategies in ASD.

Dissociating hyperactivity from impulsivity in *Cntnap2* KO mice

As *Cntnap2* KO mice display well-documented hyperlocomotion (***Peñagarikano et al., 2011***; ***Figure 1—figure supplement 1D***), a general increase in motor output represents a potential confound for several of the behavioral readouts in this study. We addressed this directly for the TFC paradigm, where resting time did not differ between genotypes despite increased total distance and velocity in the open field (***Figure 1—figure supplement 1D***), and where freezing levels during acquisition were

comparable across trace intervals and genotypes (***Figure 1—figure supplement 1A***). These findings indicate that the genotype-specific loss of retention at the 40 s trace interval reflects a deficit in temporal binding rather than an inability to freeze.

However, in the R/DM task our data more directly implicate impulsivity, rather than hyperactivity, as a contributing factor to task performance. *Cntnap2* KO mice showed shorter decision latencies specifically at the choice point of the maze (***Figure 2G***), and, critically, this latency reduction was similar regardless of whether the eventual choice was correct or incorrect. In contrast, WT mice took longer to enter non-baited arms, consistent with deliberation over reward location before committing to a choice. This pattern is consistent with premature, automatic responding rather than a general increase in locomotor drive: KO mice were in fact slower once a choice had been made (*i.e.* longer runtimes on both incorrect and correct trials; ***Figure 2H***), arguing against a simple speed-accuracy effect driven by hyperactivity.

This distinction is conceptually important, as impulsivity, characterized by premature responding and reduced response control, is a well-documented feature of ASD in both clinical and preclinical settings (DSM-5 and ***Association American Psychiatric, 2013***), including in other autism-relevant mouse models assessed with operant impulse-control paradigms. Examples include the five-choice serial reaction time task (CSRTT), where increased premature responding has been reported independently of general locomotor activity (***McTighe et al., 2013***). We therefore interpret the shortened decision latencies in *Cntnap2* KO mice as reflecting reduced deliberative evaluation of spatial/reward information prior to responding, which may compound, but is dissociable from, the reduced hippocampal engagement and egocentric strategy bias described above.

We note, however, that our task was not designed to formally quantify impulsivity (e.g. via premature responses during an imposed delay, as in the 5-CSRTT), and future studies directly assessing response inhibition in *Cntnap2* KO mice will be required to determine whether this impulsive-like phenotype is mechanistically linked to, or independent of, dCA1 hypofunction.

Aged-like performance in *Cntnap2* KO mice suggests early cognitive decline

In this study, we demonstrate the disruption in hippocampal and CA1 functioning in the *Cntnap2* KO mice, a hallmark of memory defects observed during aging (***Etchamendy et al., 2012***; ***Leal and Yassa, 2015***). Consistent with reports suggesting that people with autism are at risk of premature cognitive aging (***Wang et al., 2024***), we have found that young adult *Cntnap2* KO mice exhibit a memory profile similar to those of aged WT mice (***Al Abed et al., 2020b***; ***Marighetto et al., 2011***; ***Sellami et al., 2017***). Compared to young WT mice, both groups showed flexibility impairments in the relational/declarative radial maze task, and both exhibited a striatum-biased learning strategy. However, the underlying mechanisms driving these deficits remain unknown.

We previously demonstrated that dCA1 activity during the temporal gaps is necessary to link separate pairs into a relational/flexible memory (***Al Abed et al., 2020b***; ***Sellami et al., 2017***) and that targeted dCA1 optogenetic activation during these intervals increases temporal binding capacity, rescuing relational/declarative memory formation. Given that CA1 neurons are less synchronized in ASD, targeted dCA1 activation could alleviate memory deficits. We propose that fine-tuning dCA1 activity may normalize memory system balance, offering a novel therapeutic approach for cognitive impairments in ASD. Further delineation of associated connectomes (***Hollunder et al., 2024***) could provide insights into targeted brain circuit therapies.

Autism is a highly heterogeneous condition, with individuals presenting a wide range of atypical cognitive abilities. Consequently, the extent and nature of memory deficits vary considerably across the spectrum. Research has yet to fully elucidate how these deficits manifest, particularly in relation to other cognitive domains such as attention, executive functioning, and language. Sex differences are another factor to consider (***Van Wijngaarden-Cremers et al., 2014***). While this study included both male and female mice, we did not observe sex-specific effects, suggesting that the behavioral and cognitive phenotypes examined in the *Cntnap2* KO mouse model are largely independent of sex. This is consistent with previous studies reporting no robust sex differences (***Al Abed et al., 2024***).

A better understanding of these individual differences is necessary to create more personalized and effective interventions. As such, further studies will have to assess these aspects in different models to fully comprehend the common cognitive mechanisms at play in autism.

Materials and methods

Key resources table

Reagent type (species) or resource	Designation	Source or reference	Identifiers	Additional information
Strain, strain background (*Mus musculus*)	B6.129(Cg)-*Cntnap2*^{tm1Pele}/J	Jackson	#017482; RRID:IMSR_JAX:017482	Males and females
Strain, strain background (Adeno-associated Virus)	*AAV5-pCaMKIIα-ArchT-GFP*	UNC Vector Core	RRID:Addgene_99039-AAV5	
Strain, strain background (Adeno-associated Virus)	*AAV5-pCaMKIIα-ChR2 (H134R)-EYFP*	UNC Vector Core	RRID:Addgene_26969	
Strain, strain background (Adeno-associated Virus)	*AAV5-pCaMKIIα-GFP*	UNC Vector Core	RRID:Addgene_50469	
Strain, strain background (Adeno-associated Virus)	*AAV1-hsynjGCaMP6f-WPRE*	Addgene	RRID:Addgene_100837	
Antibody	Mouse monoclonal anti-cFos	Santa Cruz	SC166940; RRID:AB_2106783	1:1000
Antibody	Mouse polyclonal anti-Biotin	Vector Laboratories	BA-2000; RRID:AB_2313581	1:200
Antibody, fluorophore	Streptavidin 647	Jackson	016-600-084; RRID:AB_2341101	1:200
Software, algorithm	Statview	N/A	N/A	
Software, algorithm	Fiji	ImageJ	https://imagej.net/software/fiji/downloads	
Software, algorithm	Bonsai/Neurophotometrics		FP3002	
Software, algorithm	Qu Path		RRID:SCR_018257	
Software, algorithm	GraphPad Prism		RRID:SCR_002798	
Other	Fear Conditioning	FEAR-SHUTTLE	Fear-Shuttle - Imetronic	Behavioral apparatus
Other	Stereotactic frame	Kopf Instruments	N/A	Stereotaxic surgery apparatus
Other	Optical fiber stubs 2 mm	thorlabs	N/A	Optic fiber implants for fiberphotometry and optogenetic experiments
Other	LED driver system	Thorlabs	LEDD1B T-Cube	LED for optogenetic stimulation
Other	Fiber-Coupled LED	Thorlabs	M470F4	LED for fiberphotometry recordings
Other	vertical P10 puller	Narishige, Japan	N/A	Puller for glass pipette preparation for viral injection
Other	Glass Capillary, Borosilicate	Clarke Electromedical	GC-150F-15	Glass pipette for viral injection
Other	vibratome VT1200	LEICA	N/A	Slicer for fixed brain tissue for immunohistochemistry
Other	Slide scanner Axioscan Z1	Zeiss	N/A	Epifluorescence microscope for imaging

Mice

3- to 5-month-old naive mice were collectively housed in standard Makrolon cages, in a temperature- and humidity-controlled room under a 12 hr light/dark cycle (lights on at 07:00), with ad libitum access to food and water. We used both males and females to minimize the number of mice produced in this study. *Cntnap2*$^{+/+}$ (WT) and *Cntnap2*$^{-/-}$ (KO) mice (Jackson ID: #017482; RRID:IMSR_JAX:017482 ***Peñagarikano et al., 2011***) were non-littermate, though both lines were originally derived from breeders of the same colony and were used for behavior and histological analyses. To minimize potential differences between strains, we regularly inter-crossed the wildtype and *Cntnap2* KO colonies (i.e. every year) to generate heterozygous mice. These heterozygotes were then bred to produce either

WT or KO mice for experiments. Throughout the study, we used non-littermate mice originating from the same breeders. To ensure that observed differences between WT and *Cntnap2* KO were not influenced by this breeding strategy, we also assessed trace fear conditioning capacities in littermate mice and confirmed our findings using Het ×Het breeding experiments (***Figure 1—figure supplement 1C***).

All mice were bred in the same room, and maintained under identical husbandry and rearing conditions, including cage content, bedding, diet, and light/dark cycle. All experiments took place during the light phase. We replicated the behavioral experiments in two to four different batches. Mice were randomly attributed to experimental groups (e.g. trace conditions). Every effort was made to minimize the number of animals used and their suffering. All procedures were conducted in accordance with the European Directive for the care and use of laboratory animals (2010–63-EU) and the animals care guidelines issued by the animal experimental committee of Bordeaux University (CCEA50, agreement number A33-063-099; authorization N°21248), and from the Australian National University Animal Experimentation Ethics Committee (protocol numbers A2018/66, A2020/26, A2021/43, and A2024/362).

Trace fear conditioning task (TFC)

Apparatus

Fear conditioning behavior was performed in a Plexiglas conditioning chamber (20 × 20 × 30 cm), in a brightness of 100 lux, given access to the different visual-spatial cues in the experimental room. The floor of the chamber consisted of stainless-steel rods connected to a shock generator (Imetronic, Pessac, France).

Trace fear conditioning procedure

The box was cleaned with 70% ethanol before each trial.

During conditioning, each animal received three pairings of a tone (70 dB, 1 kHz, 30 s) and a footshock (0.3 mA, 50 Hz, 1 s). The two stimuli were separated by a trace interval of 5, 20, or 40 s, depending on the group. Each tone-shock pairing was separated by a 1 min interval.

All mice were submitted 24 hr later to the *Tone retention test* during which they were re-exposed to the tone alone in a dark and modified chamber [circular opaque white chamber cleaned with a 1% acetic acid solution; 2 min pre-tone, 2 min tone, and 2 min post-tone]. A context test was also performed 2 hr later, during which mice were re-exposed to the conditioning chamber alone for 6 min.

Animals were continuously recorded for off-line scoring of freezing, by an experimenter blinded to the experimental condition/group. Tone test was scored by two independent scorers. Freezing is defined as a lack of all movement except for respiratory-related movements. Acquisition of the TFC was measured by the progression of freezing during the tone across the three tone deliveries. 24 hr-retention of the trace association was measured during the tone test by the evolution of percentage of freezing time. Conditioned fear response to the tone was evaluated by calculating a normalized ratio between the tone and trace periods, *versus* outside these periods (i.e., Pre-Tone and Post-Tone): [(Tone +Trace)/2 - (pre-Tone+post Tone)/2] / [(Tone +Trace)/2 + (pre-Tone+post Tone)/2].

Radial-maze task of Relational/Declarative memory (R/DM)

Apparatus

We used an open eight-arm radial maze made of grey Plexiglas, automatized by videotracking (IMETRONIC – Pessac, France). The diameter of the central platform is 30 cm, and the arms are 55 cm long by 10 cm large. Each arm is equipped with a door at its entrance and a food-pellet delivery system at its end. The doors are individually controlled (raised up or dropped down) by the computerized system, which also controls pellet availability in the food tray at the end of each arm individually, according to the task. The maze is placed in an empty room containing visual cues to enable spatial discrimination.

Behavioral procedure

During the entire procedure, animals were submitted to one daily session. Prior to memory testing, animals were habituated to the apparatus over a period of 2 days during which animals were allowed

to move freely in the radial maze. To complete the session, mice had to visit each arm until its end. Choice accuracy was measured as the percentage of correct responses for each pair.

Stage 1: Acquisition of three-pair discriminations

The acquisition task consisted in learning the position of the food within the maze. Indeed, each animal was assigned three adjacent pairs of arms (pairs A, B, and C). In each pair, only one arm was baited as a food reward. The experiment is designed in a way that the left arms of pairs A and B are baited while the right arm of pair C is. In each trial, mice were given access to a pair (either pairs A, B, or C). A choice was made when the subject reached the food well of an arm; this also closed the door of the non-chosen arm. The trial was finished as soon as the animal returned to the central platform. The subject was then confined to the central platform for 20 s before the next discrimination trial began: this constituted the inter-pair interval (ITI). This interval was selected based on previous work showing that a 20 s ITI is sufficient to challenge temporal binding and reveal deficits in relational/declarative memory in this paradigm (***Sellami et al., 2018***).

Each daily session consisted of 20 consecutive trials comprising alternate presentations of pairs A, B, and C according to a pseudo-random sequence. A mouse was considered to reach criterion when its overall choice accuracy was at or above 75% over two consecutive sessions, given that performance in each of the three discrimination choices was at least 62% correct. The flexibility test task began the following day when criterion performance was reached. The lateralization index was quantified by using the absolute value of the subtraction of the performance on the left-baited pairs vs. the right-baited pairs. Lat = |((Pair A+Pair B) /2) - Pair C|. We then used the maximum lateralization over 3 consecutive days.

Stage 2: Flexibility probe of DM

In the test task, the position of the food in the maze did not change, but characteristic flexibility of DM expression was assessed by changing the way of presenting the arms. Indeed, in place of the pairs A and B, a pair AB was submitted to the mouse. The AB pair consisted of the combination of the two adjacent arms of the pairs A and B. It was the critical test of flexibility. Two other pairs were used as control: the pair C that remained unchanged ('unchanged learnt control') and pair N (=new) made of the two arms non-used in acquisition ('unlearnt control').

Fiber photometry

Surgery

Mice were injected unilaterally 4 weeks before behavioral experiments with an Adeno-Associated Virus (AAV) GCaMP6f (AAV1-hsyn-jGCaMP6f-WPRE, Addgene (RRID:SCR_002037); RRID:Addgene_100837). We used glass pipettes (tip diameter 25–35 µm) connected to a picospritzer (Parker Hannifin Corporation) into the right side of the dorsal CA1 of the hippocampus (0.1 µl/site; AP –1.8 mm; L+1.35 mm; DV –1.4 mm). Mice were then implanted with unilateral optic fiber implant (diameter: 200 µm; numerical aperture: 0.39; flat tip; Neurophotometrics). Implants were fixed to the skull with Super-Bond dental cement (Sun Medical, Shiga, Japan). Mice were perfused after experiments to confirm correct placements of fibers. Viral injections targeted the pyramidal cell layer of the dCA1.

Recordings

Data were recorded throughout the entire fear conditioning paradigm using a Neurophotometrics FP3002 system (Neurophotometrics, San Diego, CA). Briefly, 470 nm and 415 nm LED light was bandpass filtered, reflected by a dichroic mirror, and focused onto a multi-branch patch cord (Neurophotometrics, San Diego, CA) by a x20 objective lens. Alternating pulses of 470 and 415 nm light (~50 µW) were delivered at 60 Hz, and photometry signals were time-locked to behavior using a Bonsai workflow. Signals were analyzed using the Synaptech suite cloud service (MetaCell) and custom-made Python scripts (Code available at https://github.com/elisecr/fiberphotometry-analysis copy archived at ***Rawlinson, 2026***). Through the Synaptech platform, 470 and 415 signals were deinterleaved. For all experiments, the exponential delay period (the first 10 s ***Hon et al., 2025***) of the recording was removed. To correct for photobleaching, isosbestic (415 nm) signals were fit to a biexponential curve

to model the baseline signal with photobleaching. The fitted biexponential curve was then scaled to match the 470 nm signal using non-negative robust linear regress and subtracted from the 470 trace to correct for baseline drift. Traces were then Z-scored.

Experimental traces

Z-scored data were analyzed by custom Python scripts to extract calcium fluorescence traces for each experiment. For the trace fear conditioning experiments, these data were aligned to files generated by the poly fear software (Imetronic, France) '.dat' files to align the beginning of the tone and shock events to the closest millisecond in the Z-scored data. The timing of the tones and trace periods were extracted as described above to accurately align the data.

Peak finding

The threshold for peak analysis definition was set at 1.0. Peak analysis was conducted using a custom-built Python (RRID:SCR_024202) script to calculate peak frequency and amplitude. Code available at https://github.com/elisecr/fiberphotometry-analysis, copy archived at ***Rawlinson, 2026***.

Optogenetic manipulation of dCA1

Surgery

Mice were injected bilaterally 5 weeks prior to behavioral experiments with an Adeno-Associated Virus (AAV) containing the excitatory opsin channelrhodopsin targeting the pyramidal cells of dCA1 (pAAV-CaMKIIa-hChR2(H134R)-mCherry (#26975), Addgene). We used glass pipettes (tip diameter 25–35 µm) connected to a picospritzer (Parker Hannifin Corporation) into the dorsal CA1 of the hippocampus (0.2 µl/site; AP –1.8 mm; L+1.3 mm; DV –1.4 mm and AP –2.5 mm; L+2 mm; DV –1.4 mm). Mice were then implanted with bilateral optic fiber implants (AP –1.8 mm; L+1.3 mm; DV –1.3 mm; diameter: 200 µm; numerical aperture: 0.39; flat tip; Neurophotometrics). Implants were fixed to the skull with Super-Bond dental cement (Sun Medical, Shiga, Japan). Mice were perfused after experiments to confirm correct placements of fibers. Viral injections targeted the pyramidal cell layer of the dCA1.

Optogenetic manipulation during trace fear conditioning

Mice were conditioned under a 40 s trace interval condition, while dCA1 pyramidal neurons were activated during the 40 seconds of trace interval only. The light (≈3 mW per implanted fiber) was bilaterally conducted from the laser (Neurophotometrics, 450 nm; 5 Hz; 5ms laser on, 195ms laser off) to the mice via two fiber-optic patch cords (diameter, 200 µm; Doric Lenses). The tone test was performed 24 hr later; mice were tethered to the patch chord, without optogenetic manipulation.

Open field

Mice were placed in a 38.5 cm diameter circular arena and allowed free exploration for 5 min. These movements were recorded, and the mean velocity, distance traveled, and resting time were tracked and quantified using a custom MATLAB (Mathworks; RRID:SCR_001622) code as in ***Parkinson et al., 2024***.

Immunohistochemistry

Naïve (home cage) and trained (90 min after the flexibility test on Day 3 for c-Fos analysis) animals were perfused transcardially with 0.01 M PBS to eliminate blood and extraneous material, followed by 4% paraformaldehyde (PFA). Brains were postfixed for 36 hr in PFA. Tissues were sectioned at 40 µm using a Leica 1000 S vibratome and kept in a cryoprotective ethylene glycol solution at –20 °C until processed for immunofluorescence. Sections were first washed and permeabilized in PBS-Triton 0.25%; then non-specific binding sites were blocked by immersing the tissue in 10% normal donkey serum, 2% bovine serum albumin in PBS-Triton 0.25% during 2 hr. Tissues were then stained using the primary antibodies overnight: mouse anti-c-Fos (1:1000; Santa Cruz; RRID:AB_2106783). After 3 × 15 min washes, we added anti-Mouse biotin (1:200; Vector Laboratories BA-2000; RRID:AB_2313581) secondary antibody for 2 hr. After 3 × 15 min washes, slices were incubated with Streptavidin 647 for 45 min (1:200; Jackson ImmunoResearch, 016-600-084; RRID:AB_2341101). After 3x15 min washes,

slices were stained during 5 min with DAPI (5 µM; Sigma; RRID:SCR_028585), mounted on Livingstone slides, then covered with Mowiol (Sigma) and coverslip (Thermo Fisher). c-Fos staining from two to three slices per animal were imaged using a Nikon Axioscan confocal fluorescent microscope (×20 objective). Stained sections of WT and mutant mice were imaged during the same imaging session. Immunofluorescence signals were quantified using the quPath software (RRID:SCR_018257) with routine particle analysis procedures (size = 30–500; circularity = 0.30–1.00) to obtain cellular masks, divided by the area to obtain cell density per mm^2.

Statistics

Data are presented as mean ± SEM. Statistical analyses were performed using GraphPad Prism (RRID:SCR_002798) or StatView software for two-way ANOVA, followed by Bonferroni *post-hoc* test to assess two variables or more (e.g. interaction between genotype/group and performance/freezing/number of cFos +neurons) or Student's t test when assessing one variable only (two-tailed and unpaired). Sample sizes were determined by previous experience with similar research design and power calculations with a level of significance of 0.05 and a power of 0.9. Normality of the data was confirmed using the Kolmogorov–Smirnov test. Statistical significance was considered at $p<0.05$.

Acknowledgements

We thank all the personnel of The Australian Phenomics Facility and of The Neurocentre Magendie involved in mouse care. Australian National University Futures scheme, NHMRC Ideas Grant 2019416, Centre National pour la recherche scientifique (CNRS), Bordeaux University, L'institut national de la santé et de la recherche médicale (INSERM), the John Curtin School of Medical Research.

Additional information

Funding

Funder	Grant reference number	Author
Australian National University		Elise Caitlin Rawlinson Michael H McCullough Alice Shaam Al-Abed Nathalie Dehorter
Centre National de la Recherche Scientifique		Aline Marighetto
Institut National de la Santé et de la Recherche Médicale		Azza Sellami Aline Marighetto

The funders had no role in study design, data collection and interpretation, or the decision to submit the work for publication.

Author contributions

Elise Caitlin Rawlinson, Formal analysis, Investigation, Writing – original draft, Writing – review and editing; Michael Hugh McCullough, Formal analysis, Supervision; Azza Sellami, Investigation; Aline Marighetto, Conceptualization, Data curation, Formal analysis, Methodology, Writing – original draft, Writing – review and editing; Alice Shaam Al-Abed, Conceptualization, Data curation, Formal analysis, Supervision, Validation, Investigation, Visualization, Methodology, Writing – original draft, Project administration, Writing – review and editing; Nathalie Dehorter, Conceptualization, Data curation, Supervision, Funding acquisition, Methodology, Writing – original draft, Project administration, Writing – review and editing

Author ORCIDs

Elise Caitlin Rawlinson https://orcid.org/0009-0001-5915-8019
Michael Hugh McCullough https://orcid.org/0000-0001-6572-565X
Azza Sellami https://orcid.org/0000-0003-4033-9212
Aline Marighetto https://orcid.org/0000-0002-8893-278X

Alice Shaam Al-Abed https://orcid.org/0000-0002-6091-810X
Nathalie Dehorter https://orcid.org/0000-0001-7599-2866

Ethics

All procedures were conducted in accordance with the European Directive for the care and use of laboratory animals (2010-63-EU) and the animals' care guidelines issued by the animal experimental committee of Bordeaux University (CCEA50, agreement number A33-063-099; authorization N°21248), and from the Australian National University Animal Experimentation Ethics Committee (protocol numbers A2018/66, A2020/26, A2021/43, and A2024/362). Every effort was made to minimize the number of animals used and their suffering. All surgeries were performed under isoflurane anesthesia and appropriate pain management medication, under the guidance of the veterinarian team and ethics committee.

Peer review material

Version of Record:
Reviewer #2 (Public review): https://doi.org/10.7554/eLife.111851.3.sa1
Reviewer #3 (Public review): https://doi.org/10.7554/eLife.111851.3.sa2
Author response https://doi.org/10.7554/eLife.111851.3.sa3

Reviewed preprint v2
Reviewer #2 (Public review): https://doi.org/10.7554/eLife.111851.2.sa2
Reviewer #3 (Public review): https://doi.org/10.7554/eLife.111851.2.sa1
Author response: https://doi.org/10.7554/eLife.111851.2.sa0
eLife Assessment https://doi.org/10.7554/eLife.111851.2.sa3

Reviewed preprint v1
Reviewer #1 (Public review): https://doi.org/10.7554/eLife.111851.1.sa2
Reviewer #2 (Public review): https://doi.org/10.7554/eLife.111851.1.sa1
Reviewer #3 (Public review): https://doi.org/10.7554/eLife.111851.1.sa0
eLife Assessment https://doi.org/10.7554/eLife.111851.1.sa3

Additional files

Supplementary files

MDAR checklist

Source data 1. This Excel spreadsheet contains all raw data included in the article.

Data availability

Source data 1 contains the numerical data used to generate the figures. Code available at https://github.com/elisecr/fiberphotometry-analysis (copy archived at ***Rawlinson, 2026***).

References

Al Abed AS, Ducourneau EG, Bouarab C, Sellami A, Marighetto A, Desmedt A. 2020a. Preventing and treating PTSD-like memory by trauma contextualization. *Nature Communications* **11**:1–9. DOI: https://doi.org/10.1038/s41467-020-18002-w

Al Abed AS, Sellami A, Potier M, Ducourneau E, Gerbeaud-Lassau P, Brayda-Bruno L, Lamothe V, Sans N, Desmedt A, Vanhoutte P, Bennetau-Pelissero C, Trifilieff P, Marighetto A. 2020b. Age-related impairment of declarative memory: linking memorization of temporal associations to GluN2B redistribution in dorsal CA1. *Aging Cell* **19**:1–12. DOI: https://doi.org/10.1111/acel.13243

Al Abed AS, Allen TV, Ahmed NY, Sellami A, Sontani Y, Rawlinson EC, Marighetto A, Desmedt A, Dehorter N. 2024. Parvalbumin interneuron activity in autism underlies susceptibility to PTSD-like memory formation. *iScience* **27**:109747. DOI: https://doi.org/10.1016/j.isci.2024.109747, PMID: 38741709

Association American Psychiatric D. 2013. *Diagnostic and Statistical Manual of Mental Disorders: DSM-5*. American Psychiatric Association. DOI: https://doi.org/10.1176/appi.books.9780890425596

Bal VH, Kim SH, Cheong D, Lord C. 2015. Daily living skills in individuals with autism spectrum disorder from 2 to 21 years of age. *Autism* **19**:774–784. DOI: https://doi.org/10.1177/1362361315575840, PMID: 25922445

Banker SM, Gu X, Schiller D, Foss-Feig JH. 2021. Hippocampal contributions to social and cognitive deficits in autism spectrum disorder. *Trends in Neurosciences* **44**:793–807. DOI: https://doi.org/10.1016/j.tins.2021.08.005
Barrientos SA, Tiznado V. 2016. Hippocampal CA1 subregion as a context decoder. *The Journal of Neuroscience* **36**:6602–6604. DOI: https://doi.org/10.1523/JNEUROSCI.1107-16.2016, PMID: 27335394
Blanchard RJ, Flannelly KJ, Blanchard DC. 1986. Defensive behavior of laboratory and wild *Rattus norvegicus*. *Journal of Comparative Psychology* **100**:101–107. DOI: https://doi.org/10.1037/0735-7036.100.2.101, PMID: 3720282
Bowler D, Gaigg S, Lind S. 2011. Memory in autism: binding, self and brain. In: RothI, RezaieP (Eds). *Researching the Autism Spectrum: Contemporary Perspectives*. Cambridge University Press. p. 316–346. DOI: https://doi.org/10.1017/CBO9780511973918.013
Brewin CR. 2011. The nature and significance of memory disturbance in posttraumatic stress disorder. *Annual Review of Clinical Psychology* **7**:203–227. DOI: https://doi.org/10.1146/annurev-clinpsy-032210-104544, PMID: 21219190
Brunner D, Kabitzke P, He D, Cox K, Thiede L, Hanania T, Sabath E, Alexandrov V, Saxe M, Peles E, Mills A, Spooren W, Ghosh A, Feliciano P, Benedetti M, Luo Clayton A, Biemans B. 2015. Comprehensive analysis of the 16p11.2 deletion and null Cntnap2 mouse models of autism spectrum disorder. *PLOS ONE* **10**:e0134572. DOI: https://doi.org/10.1371/journal.pone.0134572, PMID: 26273832
Buonomano DV, Buzsáki G, Davachi L, Nobre AC. 2023. Time for memories. *The Journal of Neuroscience* **43**:7565–7574. DOI: https://doi.org/10.1523/JNEUROSCI.1430-23.2023, PMID: 37940593
Buzsáki G, Tingley D. 2018. Space and time: the hippocampus as a sequence generator. *Trends in Cognitive Sciences* **22**:853–869. DOI: https://doi.org/10.1016/j.tics.2018.07.006, PMID: 30266146
Caya-Bissonnette L, Naud R, Béïque JC. 2023. Cellular substrate of eligibility traces. *bioRxiv*. DOI: https://doi.org/10.1101/2023.06.29.547097
Caya-Bissonnette L, Béïque JC. 2024. Half a century legacy of long-term potentiation. *Current Biology* **34**:R640–R662. DOI: https://doi.org/10.1016/j.cub.2024.05.008, PMID: 38981433
Chang Q, Gold PE. 2003. Switching memory systems during learning: changes in patterns of brain acetylcholine release in the hippocampus and striatum in rats. *The Journal of Neuroscience* **23**:3001–3005. DOI: https://doi.org/10.1523/JNEUROSCI.23-07-03001.2003, PMID: 12684487
Chowdhury N, Quinn JJ, Fanselow MS. 2005. Dorsal hippocampus involvement in trace fear conditioning with long, but not short, trace intervals in mice. *Behavioral Neuroscience* **119**:1396–1402. DOI: https://doi.org/10.1037/0735-7044.119.5.1396, PMID: 16300446
Eichenbaum H. 2004. Hippocampus: cognitive processes and neural representations that underlie declarative memory the hippocampus serves a critical role in declarative. *Neuron* **44**:109–120. DOI: https://doi.org/10.1016/j.neuron.2004.08.028
Eichenbaum H. 2014. Time cells in the hippocampus: a new dimension for mapping memories. *Nature Reviews. Neuroscience* **15**:732–744. DOI: https://doi.org/10.1038/nrn3827, PMID: 25269553
Etchamendy N, Desmedt A, Cortes-Torrea C, Marighetto A, Jaffard R. 2003. Hippocampal lesions and discrimination performance of mice in the radial maze: sparing or impairment depending on the representational demands of the task. *Hippocampus* **13**:197–211. DOI: https://doi.org/10.1002/hipo.10055, PMID: 12699328
Etchamendy N, Konishi K, Pike GB, Marighetto A, Bohbot VD. 2012. Evidence for a virtual human analog of a rodent relational memory task: a study of aging and fMRI in young adults. *Hippocampus* **22**:869–880. DOI: https://doi.org/10.1002/hipo.20948, PMID: 21656872
Ferbinteanu J. 2016. Contributions of hippocampus and striatum to memory-guided behavior depend on past experience. *The Journal of Neuroscience* **36**:6459–6470. DOI: https://doi.org/10.1523/JNEUROSCI.0840-16.2016, PMID: 27307234
Hollunder B, Ostrem JL, Sahin IA, Rajamani N, Oxenford S, Butenko K, Neudorfer C, Reinhardt P, Zvarova P, Polosan M, Akram H, Vissani M, Zhang C, Sun B, Navratil P, Reich MM, Volkmann J, Yeh FC, Baldermann JC, Dembek TA, et al. 2024. Mapping dysfunctional circuits in the frontal cortex using deep brain stimulation. *Nature Neuroscience* **27**:573–586. DOI: https://doi.org/10.1038/s41593-024-01570-1, PMID: 38388734
Hon OJ, Neira S, Flanigan ME, Roland AV, Caira CM, Sides T, D'Ambrosio SL, Lee SI, Simpson Y, Buccini MC, Machinski S, Yu W, Boyt KM, Kash TL. 2025. Sex differences in BNST signaling and BNST CRF in fear processing. *eLife* **12**:RP89189. DOI: https://doi.org/10.7554/eLife.89189, PMID: 41348565
Jain A, Nakahata Y, Pancani T, Watabe T, Rusina P, South K, Adachi K, Yan L, Simorowski N, Furukawa H, Yasuda R. 2024. Dendritic, delayed, stochastic CaMKII activation in behavioural time scale plasticity. *Nature* **635**:151–159. DOI: https://doi.org/10.1038/s41586-024-08021-8, PMID: 39385027
Lazaro MT, Taxidis J, Shuman T, Bachmutsky I, Ikrar T, Santos R, Marcello GM, Mylavarapu A, Chandra S, Foreman A, Goli R, Tran D, Sharma N, Azhdam M, Dong H, Choe KY, Peñagarikano O, Masmanidis SC, Rácz B, Xu X, et al. 2019. Reduced prefrontal synaptic connectivity and disturbed oscillatory population dynamics in the CNTNAP2 model of autism. *Cell Reports* **27**:2567–2578. DOI: https://doi.org/10.1016/j.celrep.2019.05.006, PMID: 31141683
Leal SL, Yassa MA. 2015. Neurocognitive aging and the hippocampus across species. *Trends in Neurosciences* **38**:800–812. DOI: https://doi.org/10.1016/j.tins.2015.10.003, PMID: 26607684
Maister L, Plaisted-Grant KC. 2011. Time perception and its relationship to memory in Autism Spectrum Conditions. *Developmental Science* **14**:1311–1322. DOI: https://doi.org/10.1111/j.1467-7687.2011.01077.x, PMID: 22010891

Marighetto A, Brayda-Bruno L, Etchamendy N. 2011. Studying the impact of aging on memory systems: contribution of two behavioral models in the mouse. *Behavioral Neurobiology of Aging, Current Topics in Behavioral Neurosciences* **10**:67–89. DOI: https://doi.org/10.1007/7854_2011_151

McTighe SM, Neal SJ, Lin Q, Hughes ZA, Smith DG. 2013. The BTBR mouse model of autism spectrum disorders has learning and attentional impairments and alterations in acetylcholine and kynurenic acid in prefrontal cortex. *PLOS ONE* **8**:e62189. DOI: https://doi.org/10.1371/journal.pone.0062189, PMID: 23638000

Mingaud F, Le Moine C, Etchamendy N, Mormède C, Jaffard R, Marighetto A. 2007. The hippocampus plays a critical role at encoding discontiguous events for subsequent declarative memory expression in mice. *Hippocampus* **17**:264–270. DOI: https://doi.org/10.1002/hipo.20262, PMID: 17265459

Minor GN, Hannula DE, Gordon A, Ragland JD, Iosif AM, Solomon M. 2023. Relational memory weakness in autism despite the use of a controlled encoding task. *Frontiers in Psychology* **14**:1210259. DOI: https://doi.org/10.3389/fpsyg.2023.1210259, PMID: 37691809

Mocle AJ, Ramsaran AI, Jacob AD, Rashid AJ, Luchetti A, Tran LM, Richards BA, Frankland PW, Josselyn SA. 2024. Excitability mediates allocation of pre-configured ensembles to a hippocampal engram supporting contextual conditioned threat in mice. *Neuron* **112**:1487–1497. DOI: https://doi.org/10.1016/j.neuron.2024.02.007, PMID: 38447576

Parkinson RG, Xu T, Martin J, Xian Z, Ziko I, Pettitt JA, RCom-H'Cheo-Forgues A, Buckland R, Gordon SL, Parish C, Brüstle A, Dehorter N. 2024. Alpha-synuclein induced immune response triggers parkinson's disease-like symptoms. *bioRxiv*. DOI: https://doi.org/10.1101/2024.05.27.596130

Paterno R, Marafiga JR, Ramsay H, Li T, Salvati KA, Baraban SC. 2021. Hippocampal gamma and sharp-wave ripple oscillations are altered in a Cntnap2 mouse model of autism spectrum disorder. *Cell Reports* **37**:109970. DOI: https://doi.org/10.1016/j.celrep.2021.109970, PMID: 34758298

Pavlov IP. 1927. Conditioned reflexes: an investigation of the physiological activity of the cerebral cortex. *Annals of Neurosciences* **17**:136. DOI: https://doi.org/10.5214/ans.0972-7531.1017309, PMID: 25205891

Peñagarikano O, Abrahams BS, Herman EI, Winden KD, Gdalyahu A, Dong H, Sonnenblick LI, Gruver R, Almajano J, Bragin A, Golshani P, Trachtenberg JT, Peles E, Geschwind DH. 2011. Absence of CNTNAP2 leads to epilepsy, neuronal migration abnormalities, and core autism-related deficits. *Cell* **147**:235–246. DOI: https://doi.org/10.1016/j.cell.2011.08.040, PMID: 21962519

Peñagarikano O, Geschwind DH. 2012. What does CNTNAP2 reveal about autism spectrum disorder? *Trends in Molecular Medicine* **18**:156–163. DOI: https://doi.org/10.1016/j.molmed.2012.01.003, PMID: 22365836

Rashid AJ, Yan C, Mercaldo V, Hsiang H-LL, Park S, Cole CJ, De Cristofaro A, Yu J, Ramakrishnan C, Lee SY, Deisseroth K, Frankland PW, Josselyn SA. 2016. Competition between engrams influences fear memory formation and recall. *Science* **353**:383–387. DOI: https://doi.org/10.1126/science.aaf0594, PMID: 27463673

Rawlinson E. 2026. Fiberphotometry-analysis. swh:1:rev:cfe47cdb5421744eea53e0c261e12ff09eda4914. Software Heriatge. https://archive.softwareheritage.org/swh:1:dir:a46428ab7d85634cbaec883404f7c1957b2bc04f;origin=https://github.com/elisecr/fiberphotometry-analysis;visit=swh:1:snp:80d74ce65b58e88d01041957d9e2c3444bda5ae0;anchor=swh:1:rev:cfe47cdb5421744eea53e0c261e12ff09eda4914

Ring M, Gaigg SB, Altgassen M, Barr P, Bowler DM. 2018. Allocentric versus egocentric spatial memory in adults with autism spectrum disorder. *Journal of Autism and Developmental Disorders* **48**:2101–2111. DOI: https://doi.org/10.1007/s10803-018-3465-5, PMID: 29380269

Rumball F, Happé F, Grey N. 2020. Experience of trauma and PTSD symptoms in autistic adults: risk of PTSD development following DSM-5 and Non-DSM-5 traumatic life events. *Autism Research* **13**:2122–2132. DOI: https://doi.org/10.1002/aur.2306, PMID: 32319731

Scott R, Sánchez-Aguilera A, van Elst K, Lim L, Dehorter N, Bae SE, Bartolini G, Peles E, Kas MJH, Bruining H, Marín O. 2019. Loss of Cntnap2 causes axonal excitability deficits, developmental delay in cortical myelination, and abnormal stereotyped motor behavior. *Cerebral Cortex* **29**:586–597. DOI: https://doi.org/10.1093/cercor/bhx341, PMID: 29300891

Selimbeyoglu A, Kim CK, Inoue M, Lee SY, Hong ASO, Kauvar I, Ramakrishnan C, Fenno LE, Davidson TJ, Wright M, Deisseroth K. 2017. Modulation of prefrontal cortex excitation/inhibition balance rescues social behavior in *CNTNAP2*-deficient mice. *Science Translational Medicine* **9**:eaah6733. DOI: https://doi.org/10.1126/scitranslmed.aah6733, PMID: 28768803

Sellami A, Al Abed AS, Brayda-Bruno L, Etchamendy N, Valério S, Oulé M, Pantaléon L, Lamothe V, Potier M, Bernard K, Jabourian M, Herry C, Mons N, Piazza PV, Eichenbaum H, Marighetto A. 2017. Temporal binding function of dorsal CA1 is critical for declarative memory formation. *PNAS* **114**:10262–10267. DOI: https://doi.org/10.1073/pnas.1619657114

Sellami A, Abed ASA, Brayda-Bruno L, Etchamendy N, Valério S, Oulé M, Pantaléon L, Lamothe V, Potier M, Bernard K, Jabourian M, Herry C, Mons N, Marighetto A. 2018. Protocols to study declarative memory formation in mice and humans:optogenetics and translational behavioral approaches. *BIO-PROTOCOL* **8**:e2888. DOI: https://doi.org/10.21769/BioProtoc.2888, PMID: 34285997

Simon DM, Wallace MT. 2016. Dysfunction of sensory oscillations in Autism Spectrum Disorder. *Neuroscience and Biobehavioral Reviews* **68**:848–861. DOI: https://doi.org/10.1016/j.neubiorev.2016.07.016, PMID: 27451342

Tsien JZ, Huerta PT, Tonegawa S. 1996. The essential role of hippocampal CA1 NMDA receptor-dependent synaptic plasticity in spatial memory. *Cell* **87**:1327–1338. DOI: https://doi.org/10.1016/s0092-8674(00)81827-9, PMID: 8980238

Uddin LQ, Supekar K, Lynch CJ, Cheng KM, Odriozola P, Barth ME, Phillips J, Feinstein C, Abrams DA, Menon V. 2015. Brain state differentiation and behavioral inflexibility in autism. *Cerebral Cortex* **25**:4740–4747. DOI: https://doi.org/10.1093/cercor/bhu161, PMID: 25073720

Van Wijngaarden-Cremers PJM, van Eeten E, Groen WB, Van Deurzen PA, Oosterling IJ, Van der Gaag RJ. 2014. Gender and age differences in the core triad of impairments in autism spectrum disorders: a systematic review and meta-analysis. *Journal of Autism and Developmental Disorders* **44**:627–635. DOI: https://doi.org/10.1007/s10803-013-1913-9, PMID: 23989936

Vogel DHV, Jording M, Esser C, Conrad A, Weiss PH, Vogeley K. 2022. Temporal binding of social events less pronounced in individuals with Autism Spectrum Disorder. *Scientific Reports* **12**:14853. DOI: https://doi.org/10.1038/s41598-022-19309-y, PMID: 36050371

Wang J, Christensen D, Coombes SA, Wang Z. 2024. Cognitive and brain morphological deviations in middle-to-old aged autistic adults: a systematic review and meta-analysis. *Neuroscience and Biobehavioral Reviews* **163**:105782. DOI: https://doi.org/10.1016/j.neubiorev.2024.105782, PMID: 38944227

White NM, McDonald RJ. 2002. Multiple parallel memory systems in the brain of the rat. *Neurobiology of Learning and Memory* **77**:125–184. DOI: https://doi.org/10.1006/nlme.2001.4008, PMID: 11848717

Zhang L, Chen P, Schafer M, Zheng S, Chen L, Wang S, Liang Q, Qi Q, Zhang Y, Huang R. 2022. A specific brain network for a social map in the human brain. *Scientific Reports* **12**:35110581. DOI: https://doi.org/10.1038/s41598-022-05601-4, PMID: 35110581